NANO LETTERS

2009
Vol. 9, No. 8
3012-3015

Size and Chirality Dependent Elastic Properties of Graphene Nanoribbons under Uniaxial Tension

H. Zhao, K. Min, and N. R. Aluru*

Department of Mechanical Science and Engineering, Beckman Institute for Advanced Science and Technology, University of Illinois at Urbana-Champaign, Urbana, Illinois 61801

Received May 6, 2009; Revised Manuscript Received July 14, 2009

ABSTRACT

We investigate the mechanical strength and properties of graphene under uniaxial tensile test as a function of size and chirality using the orthogonal tight-binding method and molecular dynamics simulations with the AIREBO potential. Our results on Young's modulus, fracture strain, and fracture strength of bulk graphene are in reasonable agreement with the recently published experimental data. Our results indicate that fracture strain and fracture strength of bulk graphene under uniaxial tension can have a significant dependence on the chirality. Mechanical properties such as Young's modulus and Poisson's ratio can depend strongly on the size and chirality of the graphene nanoribbon.

Graphene—defined as the monolayer of honeycomb lattice packed with carbon atoms—has gained significant attention recently after experiments showed its two-dimensional lattice stability[1] and sophisticated low-dimensional electronic properties.[2,3] Many possible applications of graphene, especially as electronic devices, have already been reported.[4,5] Graphene has also been shown to possess exceptional mechanical properties[6] and many potential applications of graphene as micro- and nanoelectromechanical devices are only starting to emerge. The mechanical properties of graphene have been investigated using experimental and theoretical approaches. On the experimental side, Blakslee et al.[7] reported the Young's modulus of bulk graphite to be 1.06 ± 0.02 TPa. Recently, Frank et al.[8] measured the Young's modulus of a stack of graphene sheets (less than five layers) to be 0.5 TPa. Gomez-Navarro et al.[9] used the tip-induced deformation method to estimate the Young's modulus of a monolayer graphene oxide as 0.25 ± 0.15 TPa assuming the thickness as 1.0 nm. More recently, by nanoindenting the center of a free-standing monolayer graphene membrane with an atomic force microscope, Lee et al.[6] measured the Young's modulus as 1.0 ± 0.1 TPa assuming the thickness of graphene to be 0.335 nm. They also reported the intrinsic breaking strength of graphene as 130 ± 10 GPa. Many theoretical and computational studies have been performed to investigate the mechanical properties of graphene. By using density functional theory with a local density approximation, Liu et al.[10] computed the Young's modulus and Poisson's ratio of graphene as 1.050 TPa and 0.186, respectively. Liu et al. also reported the maximum Cauchy stress for a uniaxial tensile test in the armchair and zigzag direction (see Figure 1) to be 110 and 121 GPa, respectively. Various ab initio calculations on graphene reported either the Young's modulus (Y) values of 1.11 TPa[11] and 1.24 ± 0.01 TPa[12] assuming the thickness of graphene as $t = 0.34$ nm or the second derivative of strain energy with respect to the axial strain, $\partial^2 U/\partial\varepsilon^2$, as 57.3[13] and 60 eV,[14] without making any assumption on the graphene thickness. By using the semiempirical nonorthogonal tight-binding (TB) method, Hernandez et al.[15] reported the Young's modulus of graphene to be 1.206 TPa. Molecular Dynamics (MD) simulation has also been used to compute the mechanical properties of graphene. For example, Young's modulus of graphene was computed to be 1.272 TPa[16] with the modified Brenner potential and 1.026 TPa[17] with reactive empirical bond order (REBO) potential.

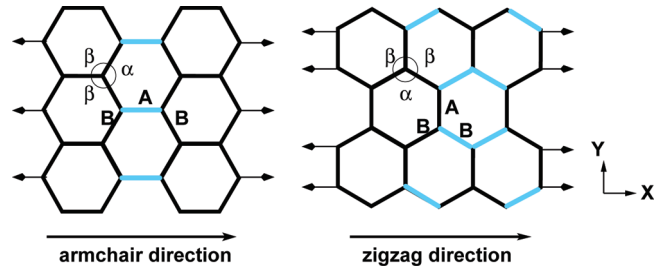

Figure 1. A graphene nanoribbon with armchair edges and zigzag edges. A uniaxial tensile test in the armchair direction refers to the figure on the left and the figure on the right is for a uniaxial tensile test in the zigzag direction. In the force-control method, the forces are applied on the edge atoms as shown in the figure.

* Corresponding author, aluru@illinois.edu and URL http://www.illinois.edu/~aluru.

10.1021/nl901448z CCC: $40.75
Published on Web 07/28/2009

With the molecular mechanics theory, the Young's modulus of graphene was computed as 0.945[18] and 1.06 TPa.[19] In summary, experimental and theoretical studies have consistently predicted that graphene has exceptional mechanical properties.

In this Letter, we investigate the size and chirality effects on the elastic properties of graphene nanoribbons using two atomistic approaches—specifically, the molecular dynamics method with the adaptive intermolecular reactive empirical bond order (AIREBO) potential[20] and the orthogonal tight-binding method.[21] As shown in Figure 1, we investigate the mechanical properties of approximately square-shape graphene nanoribbons in both the armchair direction and the zigzag direction. In particular, we investigate the size and chirality dependence of Young's modulus and Poisson's ratio of graphene nanoribbons and chirality effects on the fracture strength of bulk graphene.

Molecular dynamics simulations are performed using LAMMPS[22] with the AIREBO potential. AIREBO potential has been shown to accurately capture the bond−bond interaction between carbon atoms as well as bond breaking and bond re-forming. In order to terminate the bond-order potential to the nearest neighbor interactions, a cutoff function is used in most empirical potentials. When the fracture process is described, where the cutoff function becomes important, spuriously high bond forces can arise with nonphysical explanations with improper cutoff functions. To avoid such issues, we set the cutoff parameter to be 2.0 Å for the REBO part of the potential, as suggested in ref 23, which is an acceptable approximation for the near-fracture regime. To study mechanical properties of graphene, we perform uniaxial tensile tests under deformation-control or force-control methods. In the deformation-control method, the applied strain rate is 0.001/ps. The strain increment is applied to the structure every 1000 time steps. In the force-control method, the force is applied on the edge atoms quasi-statically by keeping the system under equilibrium for 400 ps before each load increment of 0.1 eV/Å on each of the edge atoms. All the MD simulations are carried out at 300K with the Nose−Hoover thermostat.[24] The Velocity−Verlet time stepping scheme is used with an integration time step of 0.1 fs. In the uniaxial tensile test, the engineering (nominal) strain and the engineering (nominal) stress are defined as

$$\varepsilon_x = \frac{l_x - l_x^\circ}{l_x^\circ}, \quad \varepsilon_y = \frac{l_y - l_y^\circ}{l_y^\circ}, \quad \sigma_x = \frac{1}{V^\circ}\frac{\partial U}{\partial \varepsilon_x}$$

where l_x° and l_y° are the initial lengths of the nanoribbon in x and y directions, l_x and l_y are the strained lengths of the nanoribbon, U is the strain energy, $V^\circ = l_x^\circ l_y^\circ t$ is the initial volume of the structure, and $t = 3.35$ Å[6] is the assumed graphene thickness. The Young's modulus Y and Poisson's ratio ν in the x direction are defined via the equations

$$Y = \frac{1}{V^\circ}\frac{\partial^2 U}{\partial \varepsilon_x^2}\bigg|_{\varepsilon_x=0}, \quad \nu = -\frac{\varepsilon_y}{\varepsilon_x}$$

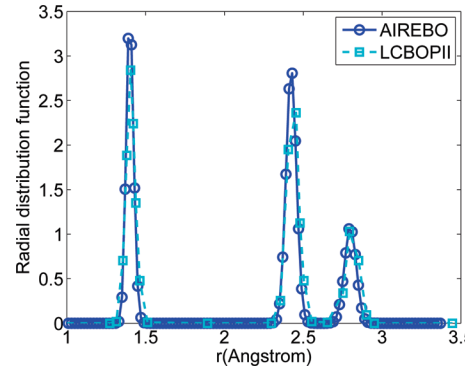

Figure 2. Comparison of the radial distribution function obtained with the AIREBO potential and the LCBOPII potential.[26]

We have also used the orthogonal tight-binding method to calculate the Young's modulus of graphene with the parameters proposed by Xu et al.[21] For a N atom system, with the relaxed atomic configuration, the total energy E can be calculated by $E = E_{bs} + E_{rep}$, where E_{bs} is the sum of electronic eigenvalues over all occupied electronic states obtained by solving an empirical tight-binding Hamiltonian, and E_{rep} is the sum of the repulsive energy calculated from the scaling function and the pairwise potential.[21] The Young's modulus of the system in the x direction can be obtained from the elastic constants[25] as (assuming graphene to be an orthotropic material)

$$\mathbf{C}_{ijkl} = \frac{\partial^2 W_T}{\partial \mathbf{E}_{ij}\partial \mathbf{E}_{kl}} - \frac{\partial^2 W_T}{\partial \mathbf{E}_{ij}\partial \boldsymbol{\xi}_m}\left(\frac{\partial^2 W_T}{\partial \boldsymbol{\xi}_m \partial \boldsymbol{\xi}_n}\right)^{-1}\frac{\partial^2 W_T}{\partial \boldsymbol{\xi}_n \partial \mathbf{E}_{kl}}$$

$$i, j, k, l, m, n = x, y, z$$

$$Y = \frac{C_{xxxx}C_{yyyy} - C_{xyxy}^2}{C_{yyyy}}$$

where $W_T = E/V^\circ$ is the energy density, V° is the initial volume of the relaxed structure, $\mathbf{E}$ is the Green−Lagrange strain tensor, and $\boldsymbol{\xi}$ is the inner displacement between the two Bravais lattices of the graphene structure.

We first investigate the equilibrium configuration of bulk graphene at room temperature by performing an NPT ensemble MD simulation of 3936 atoms (100.8 Å × 102.2 Å) with periodic boundary conditions (PBC) in the in-plane two directions. Starting with an initial random velocity for all the atoms, once the system reaches an equilibrium state, the intrinsic ripple structures can be clearly observed. We found that the typical size of the out-of-plane fluctuation is around 0.576 Å. Since the amplitude of the out-of-plane fluctuations $\bar{h}$ of a membrane with typical size L obeys the relation $\bar{h} \propto L^\zeta$ with $\zeta = 0.6-0.8$ for graphene, our estimate for the ratio $\bar{h}/L^\zeta$ is 0.036 with $\zeta = 0.6$, which is in good agreement with 0.035 calculated in ref 26. Figure 2 shows the radial distribution function of bulk graphene at 300 K calculated with AIREBO potential based MD simulations. The locations of the peaks identify the first three nearest neighbors and the distribution matches well with the published data.[26]

To investigate the effect of chirality on the mechanical properties of bulk graphene, we perform displacement-control

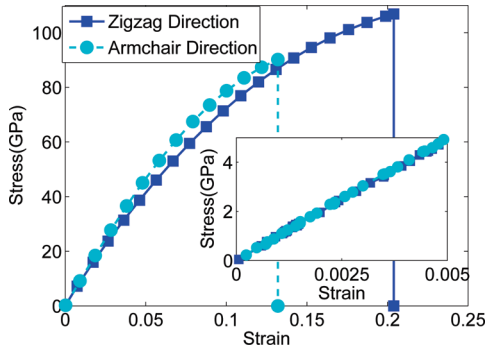

Figure 3. Stress−strain relation of bulk graphene under uniaxial tensile test in the armchair direction (dashed line with circles) and the zigzag direction (solid line with squares) at 300 K. The inset figure shows the linear elastic behavior for the small strain range without chirality effects.

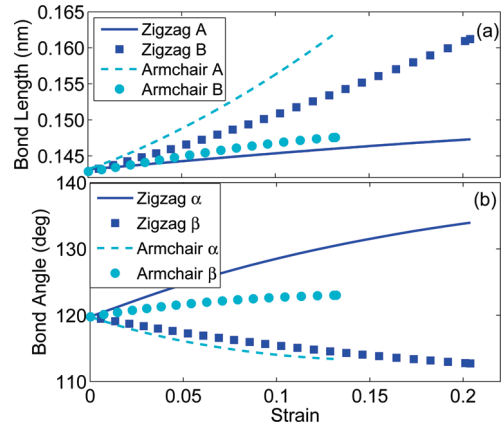

Figure 4. Variation of bond length (a) and bond angle (b) as a function of strain when uniaxial tension is applied on bulk graphene along zigzag and armchair directions. Zigzag A and Zigzag B refer to the bond lengths of type A and type B (see Figure 1) when tension is applied along the zigzag direction. Armchair A and Armchair B refer to the bond lengths of type A and type B (see Figure 1) when tension is applied along the armchair direction. Similarly, Zigzag α and Zigzag β refer to the bond angles of type α and type β (see Figure 1) when tension is applied along the zigzag direction. Armchair α and Armchair β refer to the bond angle of type α and type β (see Figure 1) when tension is applied along the armchair direction.

uniaxial tensile tests in both armchair and zigzag directions on a 3936 atom graphene lattice with PBC in the in-plane two directions. Our MD calculations indicate that 3936 atoms with PBC can accurately reproduce the mechanical properties of bulk graphene. In TB simulations, the Young's modulus in both armchair and zigzag directions is calculated using the relaxed configuration of a 680 atom graphene lattice with PBC. The Young's modulus Y_b is 1.01 ± 0.03 TPa from MD simulation and 0.91 TPa from the TB simulation. The Poisson's ratio ν_b from MD simulation is 0.21 ± 0.01. These results match with the published data quite well. Figure 3 shows the engineering strain−stress curves for uniaxial tensile tests in both armchair and zigzag directions from MD simulations. The inset of Figure 3 clearly shows the linear elastic behavior of graphene for the small strain range (<0.5%) and there is no chirality dependence for small strains. As the strain increases, the chirality dependence becomes more obvious. The fracture strain is 0.13 and 0.20 in the armchair and zigzag cases, respectively. The fracture strength, defined as the engineering stress on the material at the breaking point, is 90 and 107 GPa in the armchair and zigzag cases, respectively. The maximum Cauchy stress is 102 and 129 GPa in the armchair and zigzag cases, respectively. To understand how a graphene lattice deforms due to the tensile stress, parts (a) and (b) of Figure 4 show the variation of the bond length and bond angle with the strain in the tension direction for armchair and zigzag cases. We can clearly observe that a uniaxial tensile stress causes variations in both the bond length and the bond angle. The bonds along the tension direction (bond type A, along the armchair direction (see Figure 1)) or close to the tension direction (bond type B, 30° to the zigzag direction (see Figure 1)) undergo more deformation and are responsible for failure with very similar bond elongation at the fracture point. Furthermore, the magnitude of the bond angle variation in the zigzag direction tension test is much larger than that in the armchair direction tension test. These observations can explain why zigzag direction tension has larger fracture strain compared to the armchair direction tension. At room temperature, the brittle fracture behavior is observed in our MD simulations. The bonds with light color (shown in Figure 1) are the typical brittle fracture paths for uniaxial tensile tests in armchair and zigzag directions. For bonds that are along (or most closely aligned along) the tension direction, an expression relating the bond elongation and the elastic deformation at the brittle breaking point can be obtained by using the homogeneous deformation Cauchy−Born rule as[27]

$$\varepsilon_{bb}(\chi) = 2(\delta l/l)_{bb}[(1 - \nu) + (1 + \nu)\cos 2\chi]^{-1}$$

where ε_{bb} is the brittle breaking strain or fracture strain, $(\delta l/l)_{bb}$ is the individual bond elongation at the brittle breaking point, ν is the Poisson's ratio, and χ is the chiral angle which is equal to 0° for the armchair case and 30° for the zigzag case. Using the above equation, we estimate $\varepsilon_{bb,armchair}$:$\varepsilon_{bb,zigzag}$ = 0.66:1.00, which is consistent with our simulation results of 0.68:1.00.

To investigate the size and chirality effects on the mechanical properties of graphene nanoribbons, we perform force-control uniaxial tensile tests on approximately square-shaped graphene nanoribbons in armchair and zigzag directions with the diagonal length varying between 1.17 and 15.62 nm. MD simulations are performed using an NVT ensemble with 5.0 nm vacuum space on each side of the nanoribbon. In TB simulations, the graphene nanoribbon structures are relaxed to minimize the energy, and the Young's modulus is calculated for armchair and zigzag directions using the method described above. In parts (a) and (b) of Figure 5 we plot the variation of normalized Young's modulus Y/Y_b and normalized Poisson's ratio ν/ν_b as a function of the size of the graphene nanoribbon. We observe that Young's modulus along armchair and zigzag directions increases with the diagonal length of the nanoribbon and slowly converges to the Young's modulus of bulk graphene, whereas the Poisson's ratio decreases with the

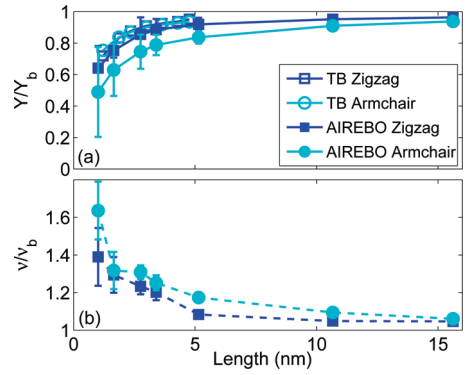

Figure 5. Normalized Young's modulus Y/Y_b (a) and normalized Poisson's ratio ν/ν_b (b) as a function of the graphene nanoribbon's diagonal length for uniaxial tension along the armchair and zigzag directions.

increase in diagonal length of nanoribbon and converges to the bulk value. This variation is similar to the size-dependent Young's modulus of a carbon nanotube, even though the Young's modulus and Poisson's ratio show more size dependence in the two-dimensional graphene nanoribbon structure compared to the one-dimensional carbon nanotube structure.[19] For example, the size effect on Young's modulus is negligible when the diagonal length of the graphene nanoribbon is over 10.0 nm. However, the size effect can be neglected when the diameter of the carbon nanotube is larger than 0.75 nm. TB simulations do not indicate any significant dependence of Young's modulus and Poisson's ratio on chirality. However, MD simulations indicate significant chirality effects. For the same size nanoribbon, Young's modulus is larger along the zigzag direction than along the armchair direction, whereas Poisson's ratio is larger in the armchair direction than in the zigzag direction. The differences in MD and TB simulation results are due to the different parameters and potentials used in the models. For instance, MD simulations are carried out at room temperature with thermal fluctuations involved in the out-of-plane direction, while TB simulations are carried out at zero-temperature with a perfect two-dimensional lattice structure. The results also suggest that potentials in MD and TB simulations need to be understood in more detail for graphene. It is also important to note that both MD and TB simulations predict similar magnitude for the size dependence, which is much larger than the prediction[28] made by the continuum mechanics approximation with the Tersoff−Brenner potential.[29] In this approach, the Young's modulus of the graphene nanoribbon is calculated based on a two-dimensional equilibrium configuration (no rippling) with the assumption of straight edges by directly minimizing the potential energy.

In summary, we have performed an extensive study to understand the size and chirality effects on the elastic properties of graphene nanoribbons. The predicted Young's modulus, Poisson's ratio, fracture strain, and fracture strength for bulk graphene are in reasonable agreement with the published theoretical[10] and experimental[6] data. In the case of bulk graphene, uniaxial tensile test along the zigzag direction has a larger fracture strain and fracture strength compared to the armchair direction. The stiffness decreases when the size of graphene nanoribbon decreases. Two-dimensional graphene nanoribbons exhibit a larger size dependence on the mechanical properties compared to the one-dimensional carbon nanotubes.

Acknowledgment. We gratefully acknowledge support by the National Science Foundation.

References

(1) Meyer, J. C.; Germ, A. K.; Katsnelson, M. I.; Novoselov, K. S.; Booth, T. J.; Roth, S. *Nature* **2007**, *446*, 60–63.
(2) Nilsson, J.; Castro Neto, A. H.; Guinea, F.; Peres, N. M. R. *Preprint at* http://arxiv.org/abs/cond-mat/0604106, 2006.
(3) Novoselov, K. S.; Geim, A. K.; Morozov, S. V.; Jiang, D.; Katsnelson, M. I.; Grigorieva, I. V.; Dubonos, S. V.; Firsov, A. A. *Nature* **2005**, *438* (7065), 197–200.
(4) Ishigami, M.; Chen, J. H.; Cullen, W. G.; Fuhrer, M. S.; Williams, E. D. *Nano Lett.* **2007**, *7* (6), 1643–1648.
(5) Schedin, F.; Geim, A. K.; Hill, E. W.; Blake, P.; Katsnelson, M. I.; Novoselov, K. S. *Nat. Mater.* **2007**, *6* (9), 652–655.
(6) Lee, C.; Wei, X.; Kysar, J. W.; Hone, J. *Science* **2008**, *321* (18), 385–388.
(7) Blakslee, O. L.; Proctor, D. G.; Seldin, E. J.; Spence, G. B.; Weng, T. *J. Appl. Phys.* **1970**, *41* (8), 3373–3382.
(8) Frank, I. W.; Tanenbaum, D. M.; van der Zande, A. M.; McEuen, P. L. *J. Vac. Sci. Technol., B* **2007**, *25* (6), 2558–2561.
(9) Gomez-Navarro, C.; Burghard, M.; Kern, K. *Nano Lett.* **2008**, *8* (7), 2045–2049.
(10) Liu, F.; Ming, P.; Li, J. *Phys. Rev. B* **2007**, *76*, 064120.
(11) Lier, G. V.; Alsenoy, C. V.; Doren, V. V.; Geerlings, P. *Chem. Phys. Lett.* **2000**, *326*, 181–185.
(12) Konstantinova, E.; Dantas, S. O.; Barone, P. M. V. B. *Phys. Rev. B* **2006**, *74*, 035417.
(13) Kudin, K. N.; Scuseria, G. E.; Yakobson, B. I. *Phys. Rev. B* **2001**, *64*, 235406.
(14) Sanchez-Portal, D.; Artacho, E.; Soler, J. M.; Rubio, A.; Ordejon, P. *Phys. Rev. B* **1999**, *59* (19), 12678–12688.
(15) Hernandex, E.; Goze, C.; Bernier, P.; Rubio, A. *Phys. Rev. Lett.* **1998**, *80* (20), 4502–4505.
(16) Gupta, S.; Dharamvir, K.; Jindal, V. K. *Phys. Rev. B* **2005**, *72*, 165428.
(17) Bao, W.; Zhu, C.; Cui, W. *Phys. B* **2004**, *352*, 156–163.
(18) Meo, M.; Rossi, M. *Compos. Sci. Technol.* **2006**, *66*, 1597–1605.
(19) Chang, T.; Gao, H. *J. Mech. Phys. Solids* **2003**, *51* (6), 1059–1074.
(20) Stuart, S. J.; Tutein, A. B.; Harrison, J. A. *J. Chem. Phys.* **2000**, *112* (14), 6472–6486.
(21) Xu, C. H.; Wang, C. Z.; Chan, C. T.; Ho, K. M. *J. Phys.: Condens. Matter* **1992**, *4* (28), 6047–6054.
(22) Plimpton, S. *J. Comput. Phys.* **1995**, *117* (1), 1–19.
(23) Shenderova, O. A.; Brenner, D. W.; Omeltchenko, A.; Su, X.; Yang, L. H. *Phys. Rev. B* **2000**, *61* (6), 3877–3888.
(24) Hoover, W. G. *Phys. Rev. A* **1985**, *31* (3), 1695–1697.
(25) Wallace, D. C. *Thermodynamics of Crystals*; John Wiley & Sons Press: New York, 1972.
(26) Fasoline, A.; Los, J. H.; Katsnelson, M. I. *Nat. Mater.* **2007**, *6* (11), 858–861.
(27) Dumitrica, T.; Hua, M.; Yakobson, B. I. *Proc. Natl. Acad. Sci. U.S.A.* **2006**, *103* (16), 6105–6109.
(28) Reddy, C. D.; Rajendran, S.; Liew, K. M. *Nanotechnology* **2006**, *17* (3), 864–870.
(29) Brenner, D. W. *Phys. Rev. B* **1990**, *42*, 9458–9471.

NL901448Z